Supporting Information

Porous Cobalt-Iron Nitride Nanowires as Excellent Bifunctional Electrocatalyst for Overall Water Splitting

Yanyong Wang, Dongdong Liu, Zhijuan Liu, Chao Xie, Jia Huo, and Shuangyin Wang*

State Key laboratory of Chem/Bio-sensing and Chemometrics, College of Chemistry and Chemical Engineering, Hunan University, Changsha, 410082, China.

Experimental details

Synthesis of Co_3Fe Double Hydroxide (Co_3Fe DH) Nanowires on Nickel Foam (NF). The Co_3Fe DH/NF precursor (denoted as Co_3Fe DH in all Figures) was synthesized by a hydrothermal reaction. In a typical experiment, nickel foam was cleaned carefully with HCl and washed with deionized water, acetone, and ethanol for several times. 5 mM iron nitrate ($Fe(NO_3)_3 \cdot 9H_2O$), 15 mM cobalt nitrate $(CoNO_3)_2 \cdot 6H_2O$) and 9.375 mM triethanolamine (TEA) were dissolved in 200 ml deionized water. Next, 7.0 mmol of urea were added to the solution and magnetically stirred for 1 h, and then a cleaned NF (3 cm × 4 cm) was immersed into the above solution for another 30 min. The solution (60 ml) and NF were transferred to a stainless-steel Teflon-lined autoclave (100 ml). After being kept in a preheated oven at 150 °C for 48 hours, the autoclave was cooled down naturally to room temperature. The Co_3Fe DH/NF precursor was washed with water and ethanol for three times and drying at 60 °C for 10 h, the Co_3Fe DH/NF nanowires precursor was obtained. Similarly, the CoFe DH/NF nanowires, Co_2Fe DH/NF nanowires and Co_4Fe DH/NF nanowires also were synthesized by the above hydrothermal reaction.

Synthesis of Co_3FeN_X/NF. In a typical experiment, a piece of Co_3Fe DH/NF was placed in a tube furnace. The furnace was heated to 300 °C, 350 °C, 400 °C respectively at 5 °C min^{-1} under a constant flowing NH_3 atmosphere (100 ml/min) and maintained for 180 min, and then cooling down naturally room temperature (denoted as Co_3Fe DH-NH3-300 °C, Co_3FeN_X and Co_3Fe DH-NH3-400 °C in all Figures, respectively). Similarly, The CoFe DH/NF nanowires, Co_2Fe DH/NF nanowires and Co_4Fe DH/NF nanowires were placed in a tube furnace which were heated 350 °C at 5 °C min^{-1} under a constant flowing NH_3 atmosphere (100 ml/min) and maintained for 180 min, and then cooling down naturally room temperature.

Synthesis of control samples. In a typical experiment, a piece of Co_3Fe DH/NF was placed in a tube furnace. The furnace was heated to 450 °C at 5 °C min^{-1} under a constant flowing Ar atmosphere (100 ml/min) and maintained for 180 min, and then cooling down naturally room temperature (denoted as Co_3Fe DH-Ar in all Figures). A piece of NF was placed in a tube furnace, which was heated to 350 °C at 5 °C min^{-1} under a constant flowing NH_3 atmosphere (100 ml/min)

and maintained for 180 min, and then cooling down naturally room temperature.(denoted as NF-NH_3 in all Figures)

Electrochemical Measurements. All of the electrochemical measurements were performed with a CHI 760D electrochemical workstation. OER and HER were performed in a three-electrode configuration and overall water splitting was performed in a two-electrode system. For electrochemical measures of OER and HER, the catalyst grown on nickel foam was used as the working electrode, saturate calomel electrode (SCE) which was constructed to a double-junction electrode to minimize contact between KOH and KCl and was used as the reference electrode in 1 M KOH electrolyte, and carbon rod was used as the counter electrode. The scan rate for linear sweep voltammetry (LSV) was kept at 2 mV/s to minimize the capacitive current. In addition, the LSV polarization curves for OER and HER was measured in saturating the solution with O_2 and H_2, respectively. In the two-electrode system for overall water splitting, the catalyst grown on nickel foam acted as the positive electrode for OER and the other catalyst grown on nickel foam acted as the negative electrode for HER. The scan rate for linear sweep voltammetry (LSV) was kept at 2 mV/s respectively. Before recording the catalytic activity, catalysts were activated by a chronopotentiometry scan with constant current density until reaching a stable state (see nature Communications, 2016, 7. Doi:10.1038/ncomms12324). All the polarization curves in this work were corrected by eliminating iR drop with respect to the ohmic resistance of the solution. Calibration of SCE reference electrodes was done by measuring the reversible hydrogen electrode (RHE) potential using a Pt electrode under a H_2 atmosphere. Amperometric i-t curve and span life measurements were performed to evaluate the long-term stability. The impedance spectra of OER and HER were measured in the three-electrode system under 1.48 V versus RHE and -0.15 V versus RHE in 1 M KOH, respectively. The Faradaic efficiency ($\mathcal{E}$) was calculated (see J. Am. Chem., 2014, 136 (39), 13925-13931) as follows:

$$\mathcal{E}=I_r/(I_d N)$$

Where I_d denotes the disk current, I_r denotes the ring current, and N denotes the current collection efficiency of the RRDE, which was determined using the same configuration with an IrO_2 thin-film electrode to be 0.21. To property calculate the Faradaic efficiency of the system, the disk electrode was held at a relatively small constant current of 200 uA; this current is sufficiently large to ensure an appreciable O_2 production and sufficiently small to minimized local saturation and bubble formation at the disk electrode.

Characterization. The morphology of all electrocatalysts was investigated by scanning electron microscope (SEM, Hitachi, S-4800) and transmission electron microscope (TEM, FEI Tecnai G20). The crystal structures of the samples were characterized using powder X-ray diffraction (XRD, Bruker D8 Advance diffractometer, Cu Kα1). The X-ray photoelectron spectroscopy (XPS) analysis was performed on an ESCALAB 250Xi X-ray photoelectron spectrometer using Mg as the excitation source. The nitrogen adsorption-desorption isotherms were measured at 77 K with a Quantachrom NOVA 1000e system. Conductivity (RTS-4, 4 probes tech). The element content was tested by ICP-OES (Optima 5300).

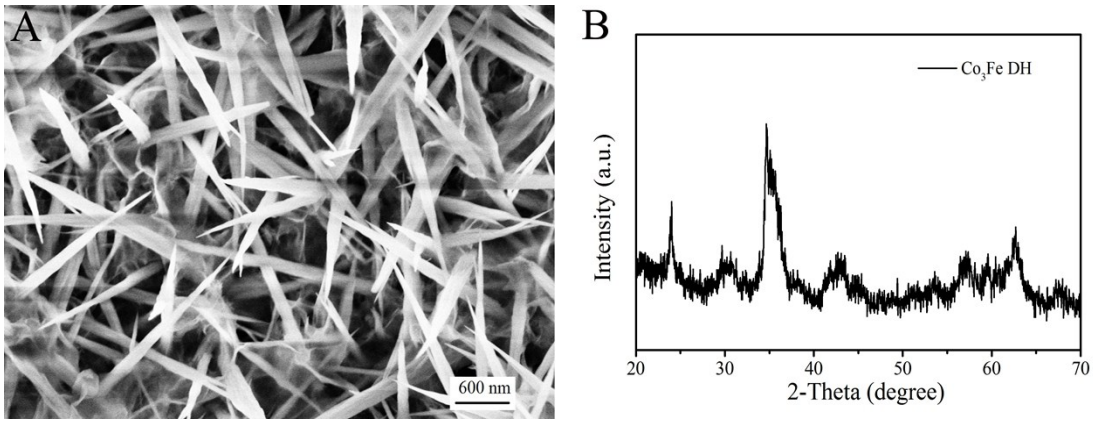

Figure S1. A) The SEM images of Co_3Fe DH/NF. B) The XRD patterns of Co_3Fe DH.

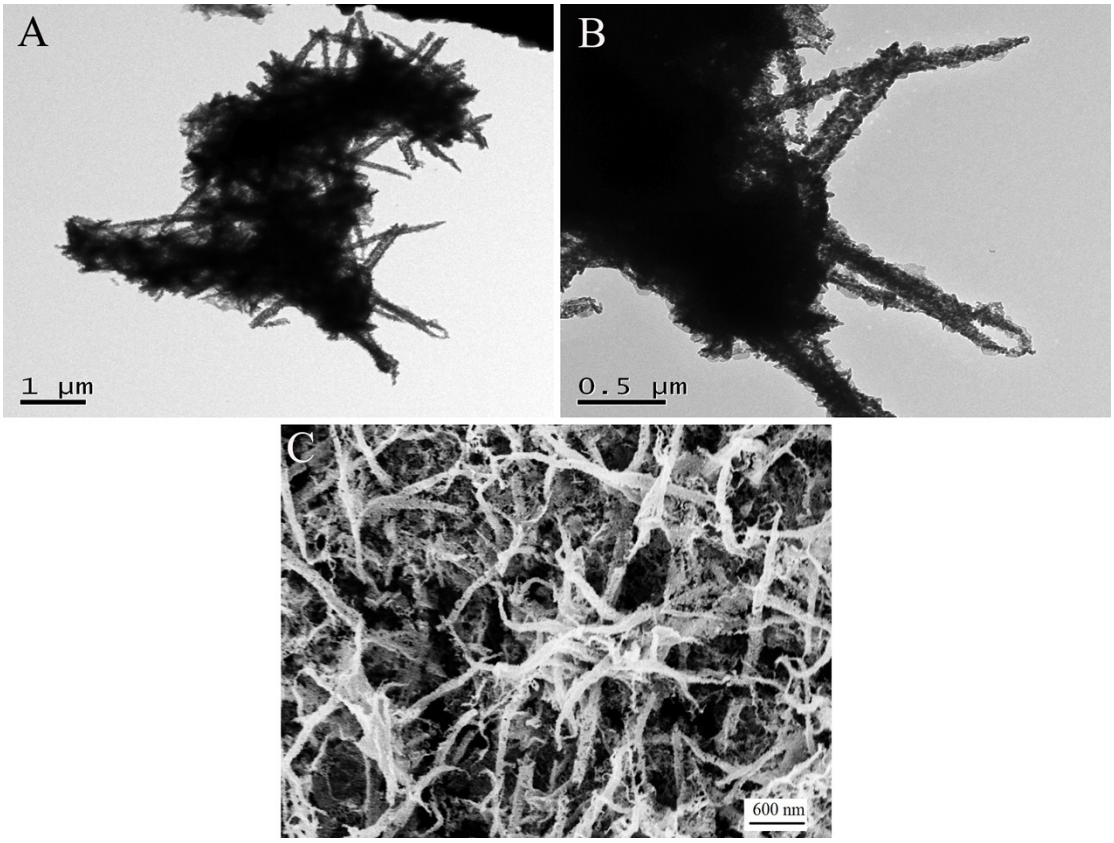

Figure S2. A) and B) The TEM images of Co_3FeN_X/NF. B) The SEM images of Co_3FeN_X/NF.

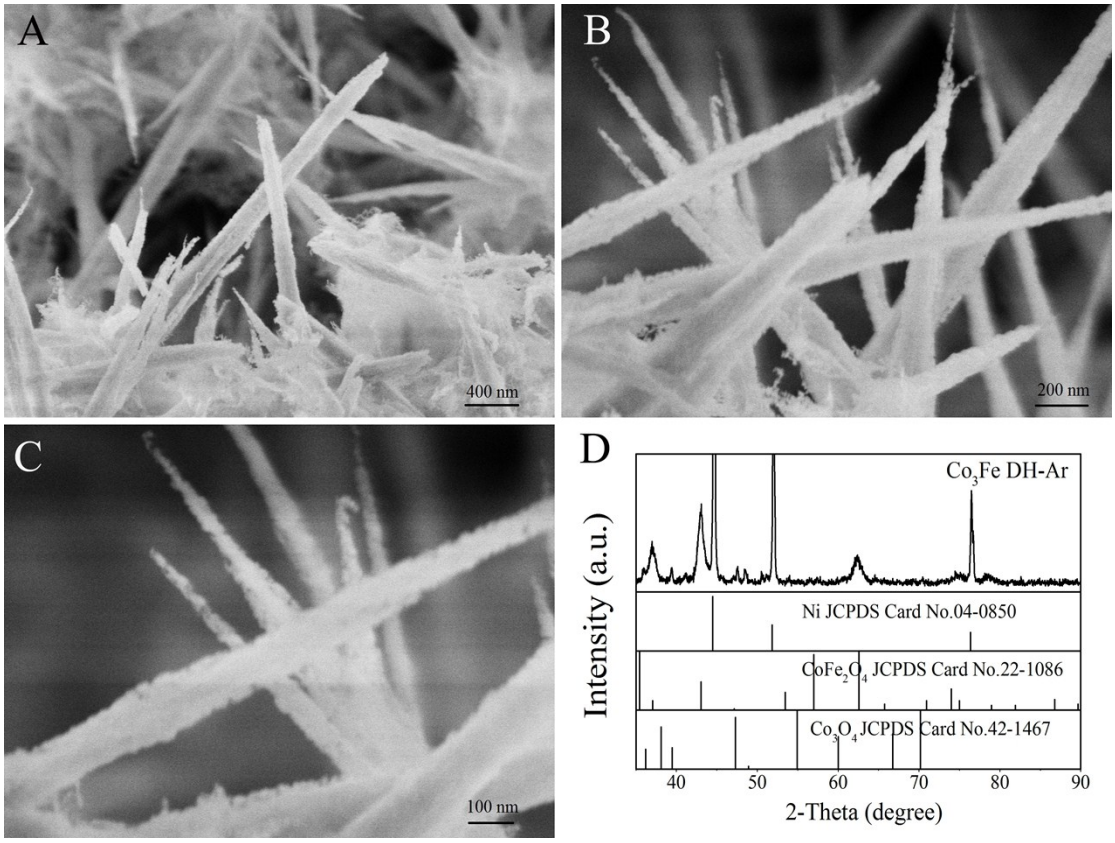

Figure S3. A), B) and C) The SEM images of Co_3Fe DH-Ar. D) The XRD patterns of Co_3Fe DH-Ar.

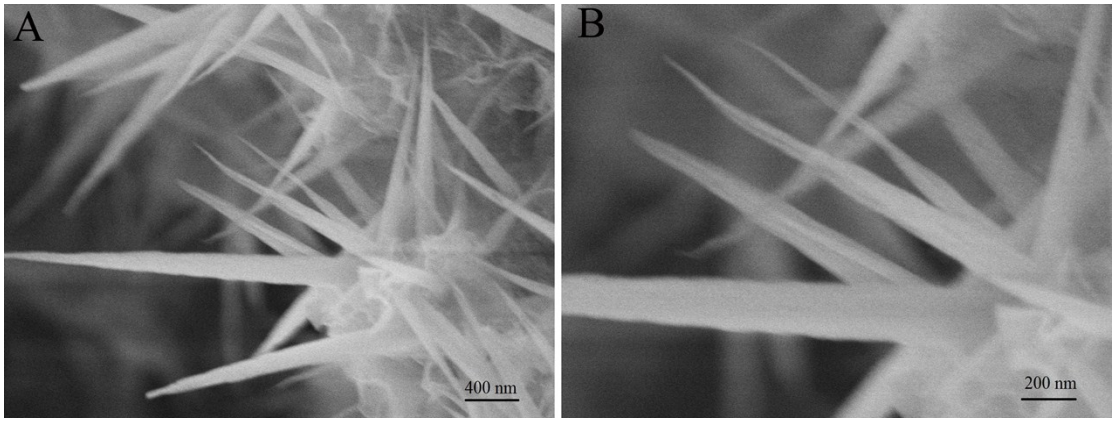

Figure S4. A) and B) The SEM images of Co_3Fe DH-NH_3-300 ℃.

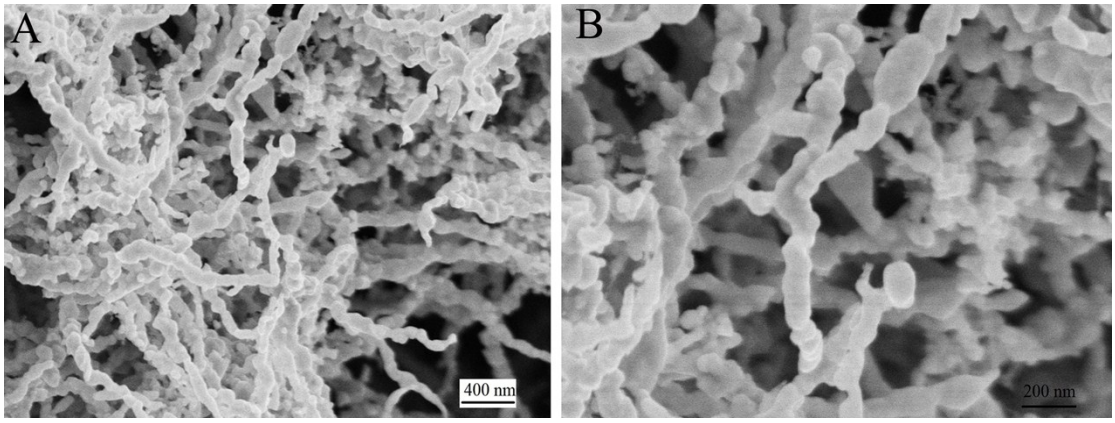

Figure S5. A) and B) The SEM images of Co_3Fe DH-NH_3-400 ℃.

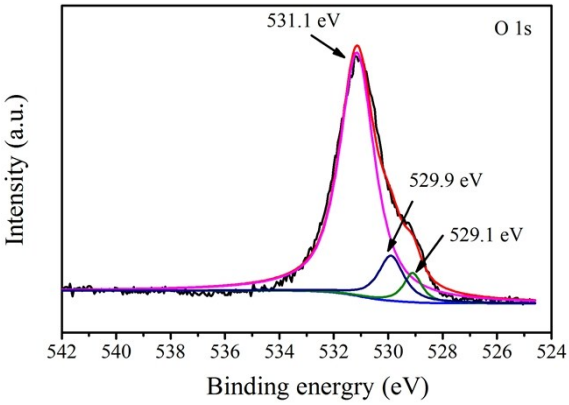

Figure S6. The O1s XPS spectrum of Co_3FeN_X. The O 1s spectrum was split into three peaks, the main peak at about 531.1 eV is ascribed to the dissociative adsorbed O_2 (see Tao H B, Fang L, Chen J, et al. Identification of Surface Reactivity Descriptor for Transition Metal Oxides in Oxygen Evolution Reaction[J]. Journal of the American Chemical Society, 2016.) and the weak peaks at 529.1 eV and 529.9 eV are ascribed to the Co-O band and Fe-O band, respectively, which can be considered to the surface oxide or oxygen doping.

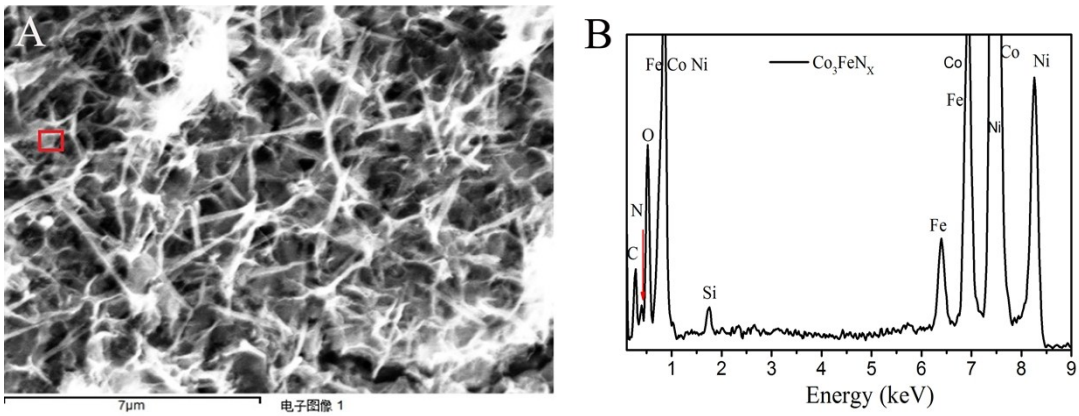

Figure S7. A) and B) The SEM and EDX images of Co_3FeN_X.

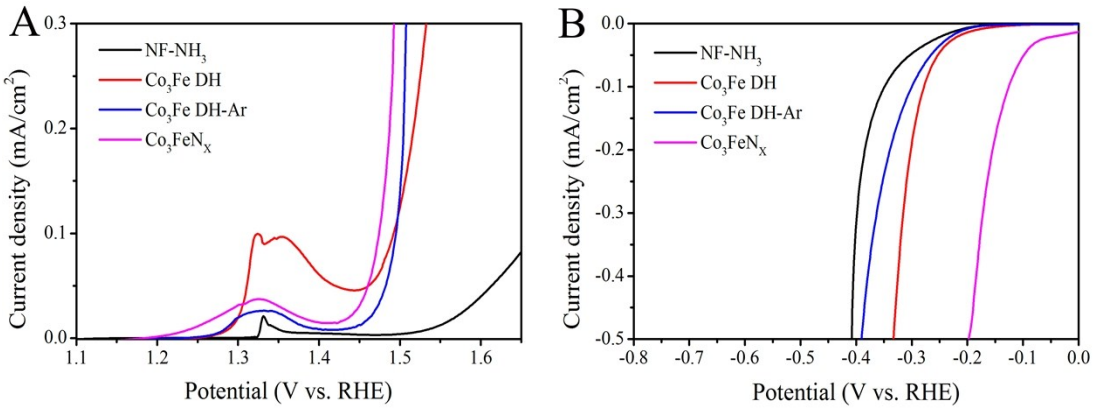

Figure S8. A) and B) The normalized current of nickel foam BET for OER and HER, respectively.

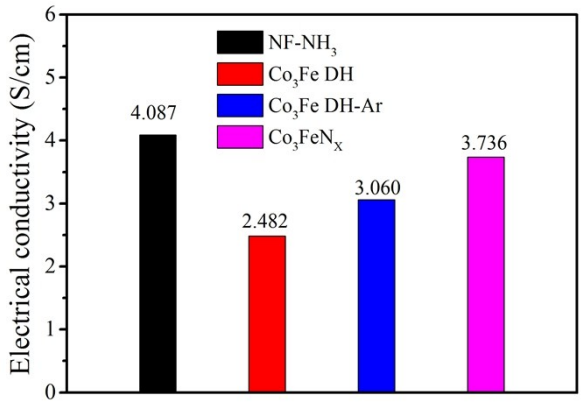

Figure S9. Electrical conductivity of the NF-NH_3, Co_3Fe DH, Co_3Fe DH-Ar, and Co_3FeN_X.

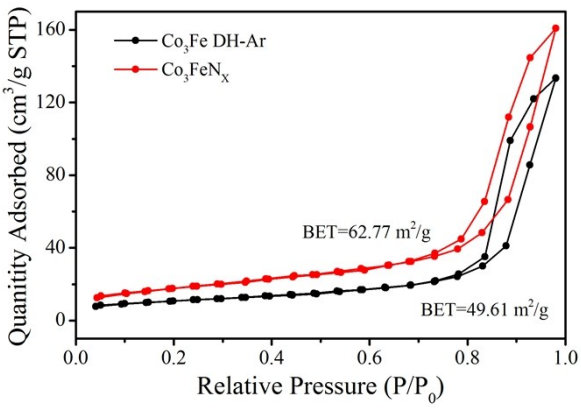

Figure S10. Nitrogen adsorption-desorption isotherms of Co_3Fe DH-Ar and Co_3FeN_X.

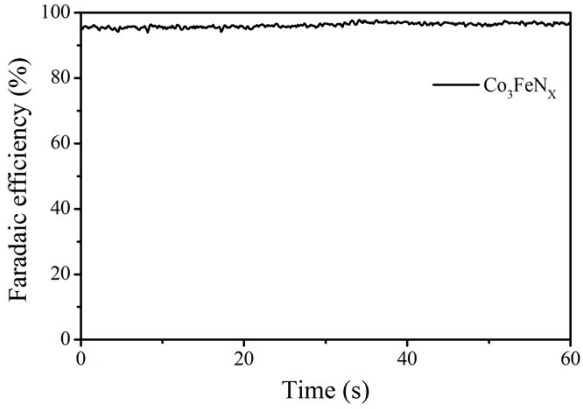

Figure S11. The Faradaic efficiency curve of Co_3FeN_X for OER.

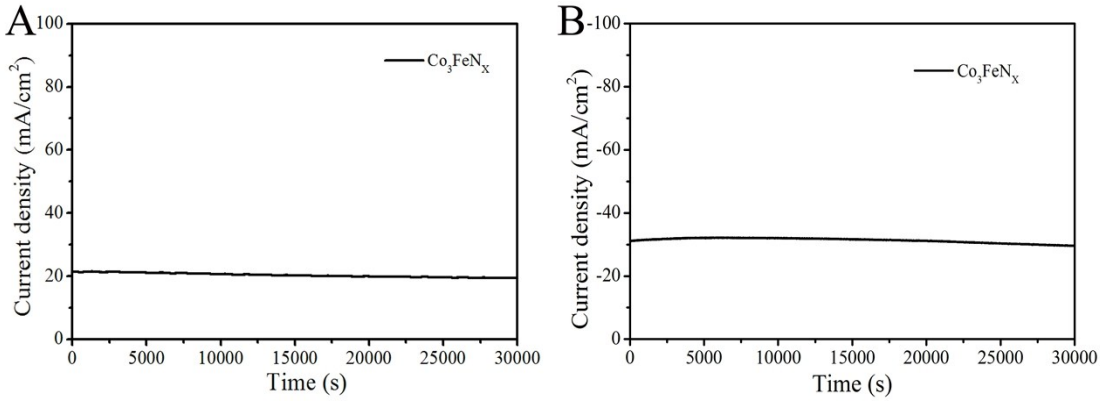

Figure S12. A) Amperometric i-t curve of Co_3FeN_x for OER at current density of about 20 mA/cm^2. B) Amperometric i-t curve of Co_3FeN_x for HER at current density of about 30 mA/cm^2.

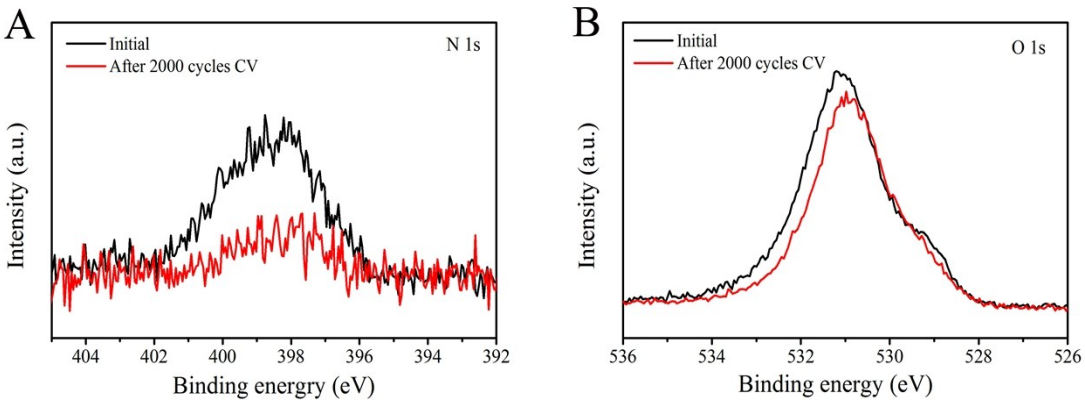

Figure S13. XPS spectra of the Co_3FeN_X and after 2000 cycles CV. A) N 1s, B) O 1s. The XPS result of N 1s shows that N 1s peak after 2000 cycles CV become weak and almost disappeared compared to initial Co_3FeN_X while O 1s peak after 2000 cycles CV has a shift towards lower binding energy, suggesting that the dissociative adsorbed O_2 content reduced and the Fe/Co-O content increased. Therefore, we hold that the surface of Co_3FeN_X was partially oxidized after 2000 cycles CV. The OER catalytic mechanism for Co-based catalysts (ref. S1) in alkaline solution have been investigated and can be depicted as follows:

$$Co^{2+} + 3OH^- \leftrightarrow CoOOH + H_2O + e^-$$

$$CoOOH + OH^- \leftrightarrow CoO(OH)_2 + e^-$$

$$CoO(OH)_2 + 2OH^- \leftrightarrow CoOO_2 + 2H_2O + 2e^-$$

$$CoOO_2 + OH^- \rightarrow CoOOH + O_2 + e^-$$

$$\text{Summary OER: } 4OH^- \rightarrow O_2 + 2H_2O + 4e^-$$

In our work, we hold that the catalytic mechanism of Co_3FeN_X/NF is similar to that of the mechanism proposed above for Co-based catalysts during the OER process in an alkaline medium. Firstly, the Co_3FeN_X/NF surface was partially oxidized to CoOOH/Co_3FeN_X/NF as the surface active sites. Secondly, with increasing of potential, CoOOH/Co_3FeN_X/NF can be oxidized to $CoOO_2$/Co_3FeN_X/NF in 1 M KOH. Finally, $CoOO_2$/Co_3FeN_X/NF is further oxidized which will lead to O_2 and CoOOH/Co_3FeN_X/NF generation.

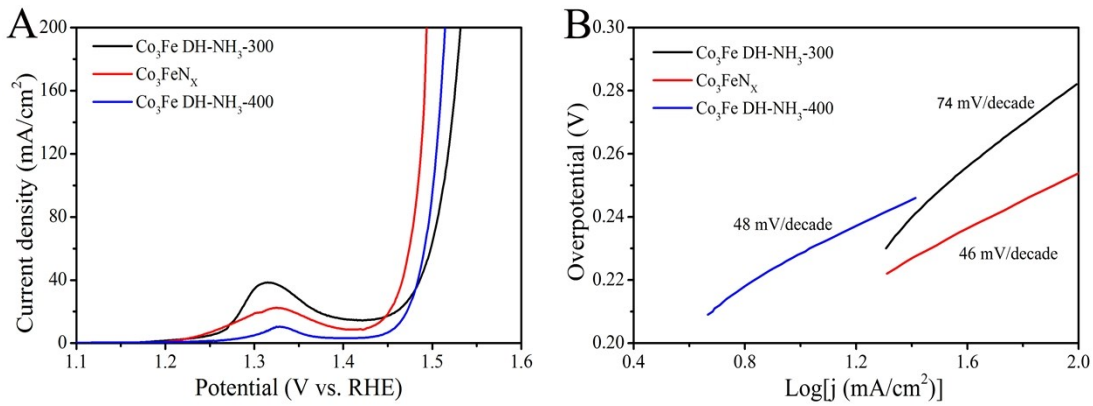

Figure S14. A) LSV curves for OER, B) Tafel plots of the Co_3Fe DHs-NH_3-300 ℃ (black curve), Co_3FeN_X (red curve), and the Co_3Fe DHs-NH_3-400 ℃(blue curve).

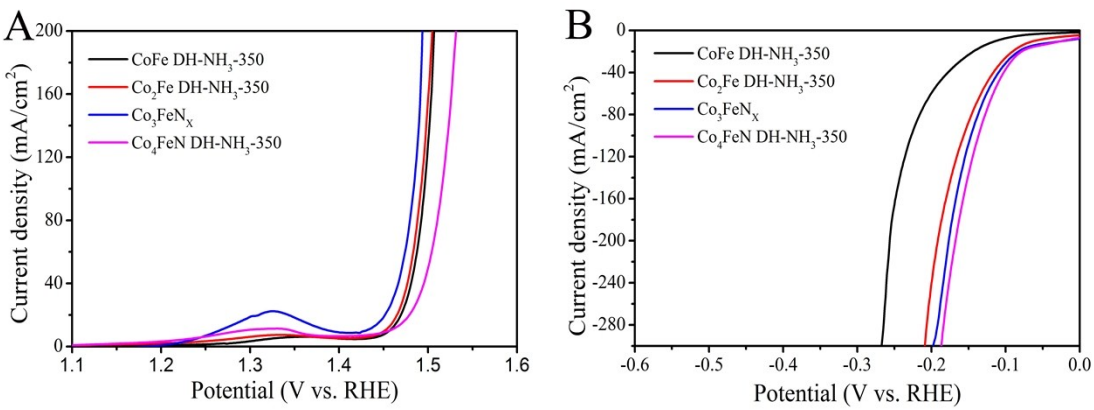

Figure S15. A) The LSV curves for OER and B) HER of the Co/Fe composition ratio from 1:1, 2:1, 3:1 to 4:1 in the precursors by NH_3 treatment at 350 ℃.

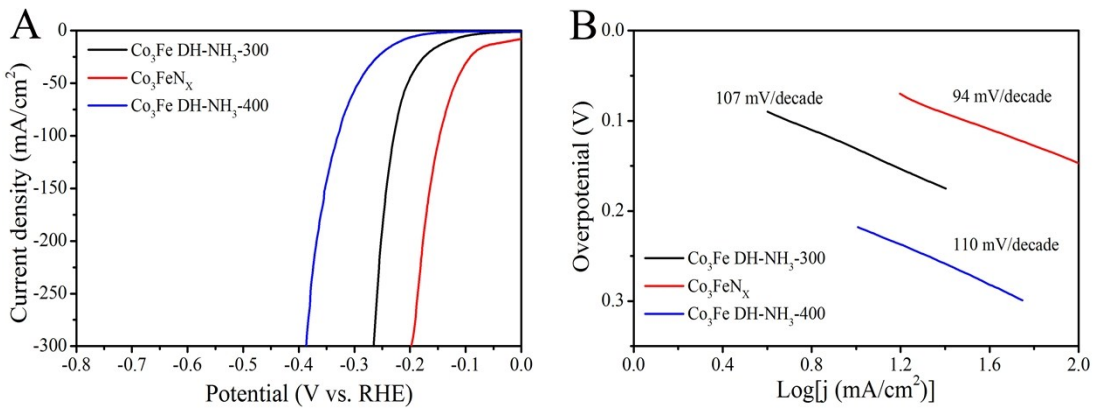

Figure S16. A) LSV curves for OER, B) Tafel plots of the Co_3Fe DHs-NH_3-300 ℃ (black curve), Co_3FeN_X (red curve), and the Co_3Fe DHs-NH_3-400 ℃(blue curve).

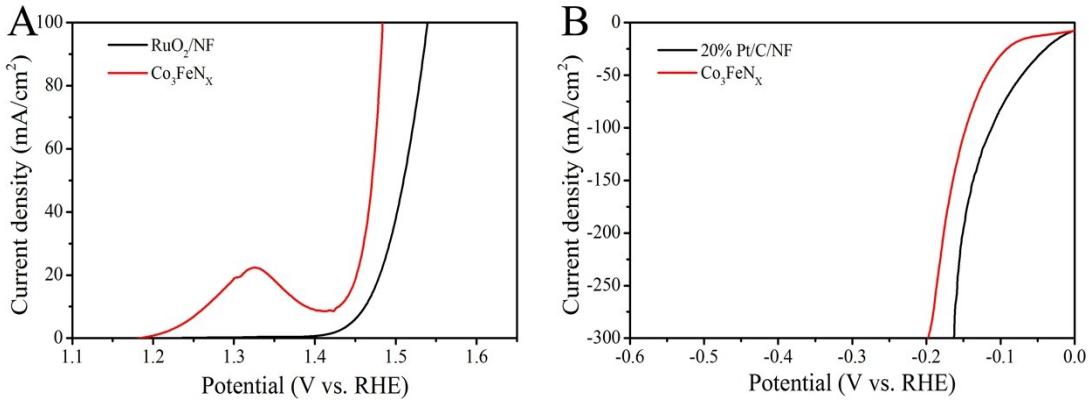

Figure S17. A) The LSV curves for OER of RuO_2 and Co_3FeN_X, B) The LSV curves for HER of 20% Pt/C, and Co_3FeN_X.

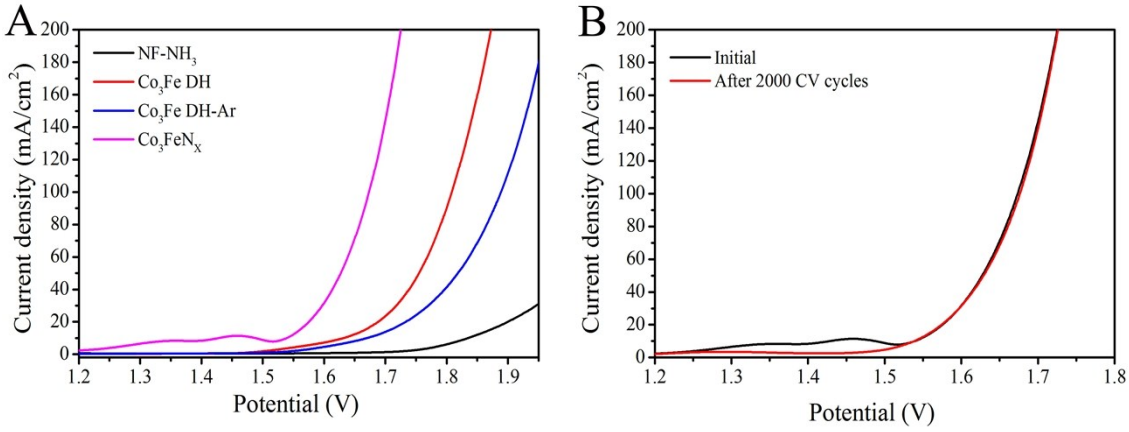

Figure S18. A) LSV curves and B) Stability test of overall water splitting for NSP-Co_3FeN_X in a two-electrode system with a scan rate of 2 mV/s.

Table S1. The weight percentage and atomic ratio of NSP-Co_3FeN_X.

NSP-Co_3FeN_X	Weight percentage (%)	The atomic ratio
Co	54.64	3
Fe	17.25	1

Table S2. Comparison of OER activity of the NSP-Co_3FeN_X/NF with recently reported catalyst.

Electrocatalyst	Electrolyte solution	Current density (mA/cm^2)	Overpotential at the corresponding Current density (mV)	Tafel slope	Reference
NSP-Co_3FeN_X/NF	1 M KOH	20	222	46	This work
		50	241		
		100	254		
SOA-Co_4N NW/CC	1 M KOH	10	257	44	Ref. S1
Co_3O_4 NW/CC	1 M KOH	10	320	72	
CoN/NF	1 M KOH	10	290	70	Ref. S2
3DG/CoAl-NSs	1 M KOH	10	252	64	Ref. S3
Co-B_i NS/G	1 M KOH	10	290	53	Ref. S4
PE-Co_3O_4 NS/Ti	0.1 M KOH	10	300	68	Ref. S5
$CoFeNiO_X$/NF	1 M KOH	10	240		Ref. S6
$NiCo_2O_4$	1 M NaOH	10	290	53	Ref. S7
$NiCo_2S_4$/NF	1 M KOH	10	260	40.1	Ref.S8
$NiCeO_X$-Au	1 M NaOH	10	271		Ref.S9
CP/CTs/Co-S	1 M KOH	10	306	72	Ref.S10

Table S3. Comparison of HER activity of the NSP-Co_3FeN_X/NF with recently reported catalyst.

Electrocatalyst	Electrolyte solution	Current density (mA/cm^2)	Overpotential at the corresponding Current density (mV)	Tafel slope	Reference
NSP-Co_3FeN_X/NF	1 M KOH	10	23	94	This work
		20	83		
		50	119		
$NiCo_2S_4$/NF	1 M KOH	10	210	59	Ref. S8
CP/CTs/Co-S	1 M KOH	10	190	131	Ref. S10
CoSe/NiFe-LDHs/EG	1 M KOH	10	260		Ref. S11
C-$CoSe_2$/CC	1 M KOH	10	190	85	Ref. S12
Ni_3S_2/NF	1 M KOH	10	223	-	Ref. S13
NiSe/NF	1 M KOH	10	96	43	Ref. S14
CoP/CC	1 M KOH	10	210	51	Ref.S15

Table S4. Comparison of the bifunctional water splitting activity of the NSP-Co_3FeN_X/NF with recently reported bifunctional catalysts in basic solutions.

Electrocatalyst	Mass loading (mg/cm^2)	Electrolyte solution	Current density ($mV \cdot mA/cm^2$)	Water splitting voltage (V)	Reference
NSP-Co_3FeN_X/NF	0.8	1 M KOH	10	1.539	This work
			20	1.575	
			50	1.628	
$NiCo_2O_4$		1 M KOH	10	1.65	Ref. S7
$NiCo_2S_4$/NF		1 M KOH	10	1.63	Ref. S8
CP/CTs/Co-S		1 M KOH	10	1.74	Ref. S10
CoSe/NiFe-LDHs/EG		1 M KOH	10	1.67	Ref. S11
Ni_3S_2/NF	1.6	1 M KOH	13	1.76	Ref. S13
NiSe/NF		1 M KOH	10	1.63	Ref. S14

REFERENCE

1. P. Chen, K. Xu, Z. Fang, Y. Tong, J. Wu, X. Lu, X. Peng, H. Ding, C. Wu and Y. Xie, *Angew. Chem.*, 2015, **127**, 14923-14927.
2. Y. Zhang, B. Ouyang, J. Xu, G. Jia, S. Chen, R. S. Rawat and H. J. Fan, *Angew. Chem. Int. Ed.*, 2016, **55**, 8670-8674.
3. J. Ping, Y. Wang, Q. Lu, B. Chen, J. Chen, Y. Huang, Q. Ma, C. Tan, J. Yang, X. Cao, Z. Wang, J. Wu, Y. Ying and H. Zhang, *Adv. Mater.*, 2016. DOI:10.1002/adma.201601019
4. P. Chen, K. Xu, T. Zhou, Y. Tong, J. Wu, H. Cheng, X. Lu, H. Ding, C. Wu and Y. Xie, *Angew. Chem. Int. Ed.*, 2016, **55**, 2488-2492.
5. L. Xu, Q. Jiang, Z. Xiao, X. Li, J. Huo, S. Wang and L. Dai, *Angew. Chem.*, 2016, **128**, 5363-5367.
6. C. G. Morales-Guio, L. Liardet and X. Hu, *J. Am. Chem. Soc.*, 2016, **138**, 8946-8957.
7. X. Gao, H. Zhang, Q. Li, X. Yu, Z. Hong, X. Zhang, C. Liang and Z. Lin, *Angew. Chem. Int. Ed.*, 2016, **55**, 6290-6294.
8. A. Sivanantham, P. Ganesan and S. Shanmugam, *Adv. Funct. Mater.*, 2016, **26**, 4660-4660.
9. J. W. D. Ng, M. García-Melchor, M. Bajdich, P. Chakthranont, C. Kirk, A. Vojvodic and T. F. Jaramillo, *Nature Energy*, 2016, **1**, 16053. DOI: 10.1038/nenergy.2016.53
10. J. Wang, H.-x. Zhong, Z.-l. Wang, F.-l. Meng and X.-b. Zhang, *ACS Nano*, 2016, **10**, 2342-2348.
11. Y. Hou, M. R. Lohe, J. Zhang, S. Liu, X. Zhuang and X. Feng, *Energy & Environmental Science*, 2016, **9**, 478-483.
12. P. Chen, K. Xu, S. Tao, T. Zhou, Y. Tong, H. Ding, L. Zhang, W. Chu, C. Wu and Y. Xie, *Adv. Mater.*, 2016. DOI: 10.1002/adma.201601663
13. L.-L. Feng, G. Yu, Y. Wu, G.-D. Li, H. Li, Y. Sun, T. Asefa, W. Chen and X. Zou, *J. Am. Chem. Soc.*, 2015, **137**, 14023-14026.
14. C. Tang, N. Cheng, Z. Pu, W. Xing and X. Sun, *Angew. Chem. Int. Ed.*, 2015, **54**, 9351-9355.
15. J. Tian, Q. Liu, A. M. Asiri and X. Sun, *J. Am. Chem. Soc.*, 2014, **136**, 7587-7590.